Seismic repeatability, normalized rms, and predictability

Ed Kragh and Phil Christie, Schlumberger Cambridge Research, Cambridge, England, U.K.

Time-lapse data are increasingly used to study production-induced changes in the seismic response of a reservoir as part of a reservoir management program. However, residual differences in the repeated time-lapse data that are independent of changes in the subsurface geology impact the effectiveness of the method. These differences depend on many factors such as signature control, streamer positioning, and recording fidelity differences between the two surveys. Such factors may be regarded as contributing to the time-lapse noise and any effort designed to improve the time-lapse signal-to-noise ratio must address the quantifiable repeatability of the seismic survey.

Although there are counter-examples (for example, Johnston et al., 2000), minimization of the acquisition footprint and repeatability of the geometry to equalize residual footprints in both surveys are considered important. This has been a key objective in the development of point receiver acquisition systems.

In this study, which develops the analysis from Kragh and Christie (2001), we examine the use of two repeatability metrics in assessing the similarity of two sets of repeat 2D lines acquired with a marine point receiver system. In one repeat set, no streamer positioning control was in use; in the other repeat set, positioning differences were minimized using the streamer positioning control.

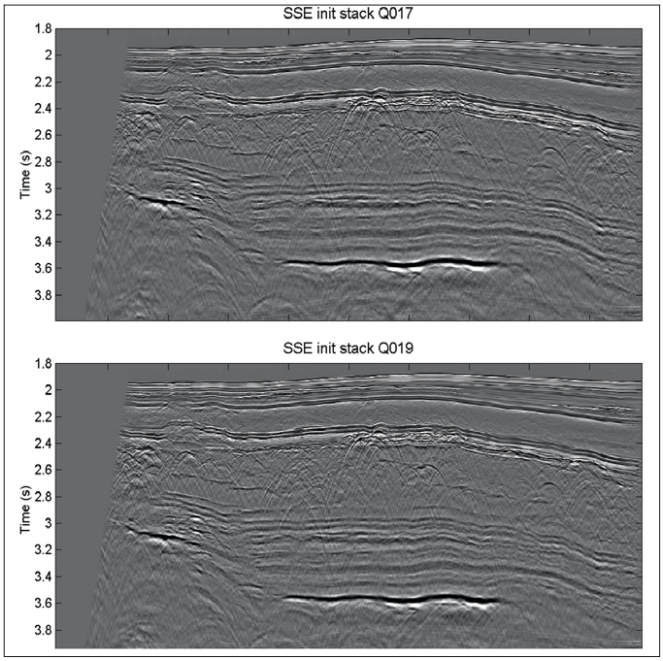

Figure 1. *Gulf of Mexico stacks. First pass (upper panel) and second pass (lower panel).*

Repeatability metrics. There does not appear to be a standard measure of repeatability, defined as a metric, to quantify the likeness of two traces. One commonly used metric is the normalized rms difference of the two traces, a_t and b_t within a given window t_1-t_2: the rms of the difference divided by the average rms of the inputs, and expressed as a percentage:

$$NRMS = \frac{200 \times RMS(a_t - b_t)}{RMS(a_t) + RMS(b_t)}$$

where the rms operator is defined as:

$$RMS(x_t) = \sqrt{\frac{\sum_{t_1}^{t_2} (x_t)^2}{N}}$$

and N is the number of samples in the interval t_1-t_2.

The values of nrms are not intuitive and are not limited to the range 0-100%. For example, if both traces contain random noise, the nrms value is 141% ($\sqrt{2}$). If both traces anticorrelate (i.e., 180° out of phase, or if one trace contains only zeros) the nrms error is 200%, the theoretical maximum. If one trace is half the amplitude of the other, the nrms error is 66.7%.

Predictability (Kristiansen et al., 2000) is another measure of repeatability and is equivalent to the coherence of White (1980), who used it to quantify the spectral match between synthetic seismograms and seismic traces as the proportion of power on the seismic trace that can be predicted by linear filtering of the synthetic trace. Here, it is defined in terms of correlations. It is the summed squared crosscorrelation within a time window divided by the summed product of the autocorrelations, expressed as a percentage:

$$PRED = \frac{\sum \Phi_{ab}(\tau) \times \Phi_{ab}(\tau)}{\sum \Phi_{aa}(\tau) \times \Phi_{bb}(\tau)}$$

where ϕ_{ab} denotes the crosscorrelation between traces a_t and b_t computed within the time window t_1-t_2. When expressed as a percentage, predictability values lie in the range 0-100%. Predictability is sensitive to the length of the correlation time window and to number of lags in the correlations, and so absolute numbers are not meaningful. In our examples, the summation intervals for the dot products are fixed at ±16 samples from zero lag. Predictability is not sensitive to overall static, phase, or amplitude differences (unlike nrms). It is sensitive to noise and to changes in the earth reflectivity. If both traces are uncorrelated, predictability is zero. If both traces anticorrelate, predictability is 100%. If one trace is half the amplitude of the other, the predictability is 100%. Conversely, nrms is extremely sensitive to the smallest of changes in the data. For example, a 10° phase shift, which is equivalent to a 0.55 ms shift at 50 Hz (or 1.1 ms at 25 Hz), gives rise to a 17.4% nrms residual.

Several authors quote values of nrms from time-lapse case studies. Koster et al. (2000) reported a typical nrms of 35% in Draugen Field where they successfully observed water replacing oil. With careful matching, Eiken et al. (1999) improved from 15% to 6% the nrms between two densely sampled surveys acquired a few days apart. Kristiansen et al. (2000) applied both metrics to the towed and seabed 4D data in Foinaven and observed that, while the seabed data

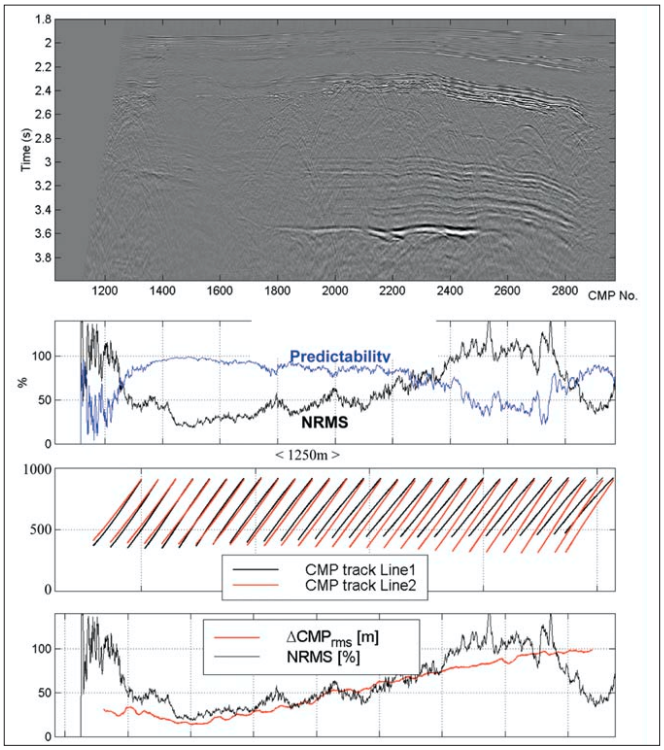

Figure 2. *Gulf of Mexico data. Top down: Difference image, nrms and predictability, CMP tracks for every 30th shot position along the line (black = first pass and red = second pass), nrms and mean midpoint error.*

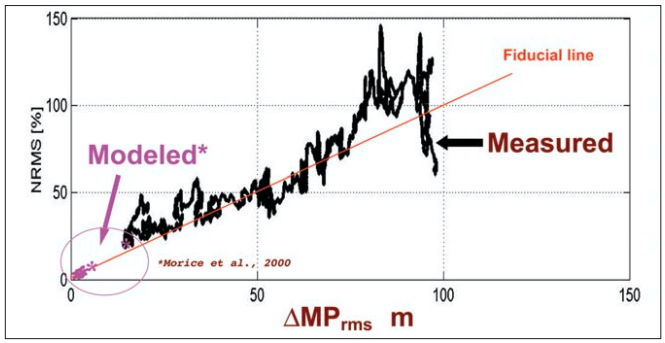

Figure 3. *Gulf of Mexico data; nrms values versus rms midpoint error. Modeled data (Morice et al., 2000), are plotted as magenta stars.*

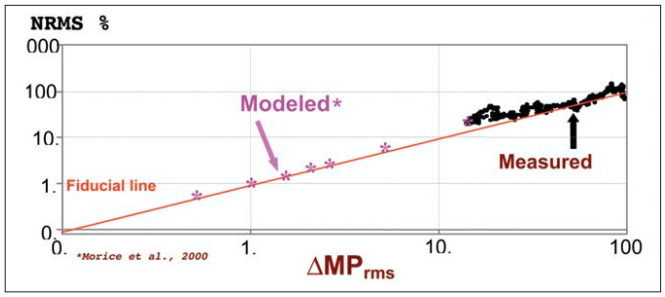

Figure 4. *Gulf of Mexico data; nrms values versus rms midpoint error, as shown in Figure 3, but plotted on a log-log axis. Modeled data (Morice et al., 2000), are plotted as magenta stars.*

sets were visually more repeatable than the towed data sets, the metrics showed a more marginal difference in predictability (93% for the towed data and 96% for the seabed data).

Data example 1, Gulf of Mexico. A repeat 2D seismic line was acquired in the Gulf of Mexico. The time interval between acquisitions was two days, and sea state was calm in both passes. Data were acquired from point receivers and processed using source signature deconvolution and digital group forming (Jenkerson et al., 2000; Özbek, 2000). The output group interval was 12.5 m. Both lines were processed identically. No active streamer positioning control was used when acquiring these data.

Figure 1 shows the first pass (upper panel) and second pass (lower panel). No migration has been performed. Figure 2 shows the difference image after subtracting the two processed stacked lines. There are clear features across much of the difference image that relate to subsurface structure. Between CMPs 1400 and 1700 the difference is much quieter; the seismic is, visually, highly repeatable. Below the seismic difference image, a number of attributes are plotted. The second panel down shows the nrms and predictability values computed for each CMP over the time window 2-4 s. There is a clear negative correlation between these two metrics. Between CMPs 1400 and 1700 (where the data appear highly repeatable), nrms values are typically 18-30% with predictability values of 99-93%. Where the data are most predictable (just over 99%), the corresponding nrms residual is just over 20%. The third panel down in Figure 2 shows CMP tracks for every 30th shot position along the line. Note that the vertical axis (cross-line offset) is highly exaggerated. The black lines show the first pass line 1, and the red lines show the second pass line 2. The plots essentially represent the streamer positions for these shots (all source locations were within 10 m, cross-line).

The data are most repeatable where the streamer positions most closely coincide, suggesting that the chief cause of the residual error is nonrepeatability of the streamer positioning. We note that, for this test, streamer positioning control (Bittleston et al., 2000) was not used and strong currents made it difficult to replicate the streamer position on the second pass. The lowest panel in Figure 2 plots the nrms values (as in the second panel down) with rms error of the midpoint locations (in meters) in red. A roughly linear correlation is evident, with the most repeatable data corresponding to rms errors in midpoint location of 15-20 m, which is mostly a cross-line error.

The Gulf of Mexico data suggest a strong correlation of nrms with the positioning error. Figure 3 shows a plot of the nrms values against the midpoint error (i.e, a plot of data in the lowest panel in Figure 2). An approximately linear correlation is evident (the magenta colored stars are modeled data explained in the following paragraph). The red line is placed fiducially to indicate this correlation. It does not represent any kind of best fit, or expectation. We would, in fact, not expect this correlation to pass through the origin, as even with zero positioning error, we would still expect some residual differences due to other sources of noise. It is possible that we can see this tail-off toward finite nrms at zero positioning error on the real data values. However, the approximate one-to-one correlation of nrms against midpoint error is clear, out to about 70 m.

It is interesting that Morice et al. (2000) also found a linear trend in the nrms errors associated with positioning errors using DMO illumination. They used a modeling approach, with typical 3D geometries, and the positioning errors they considered were much smaller than those observed in the Gulf of Mexico data (they considered errors of the size expected when streamer positioning control is in use). The results from Morice et al. (2000) are plotted on Figure 3 as the magenta-colored stars. Note that the 40-Hz modeled values are plotted, which matches the real data central frequency. The modeled data lie almost exactly on the fiducial line. Figure 4 shows exactly the same data but plotted on a log-log scale.

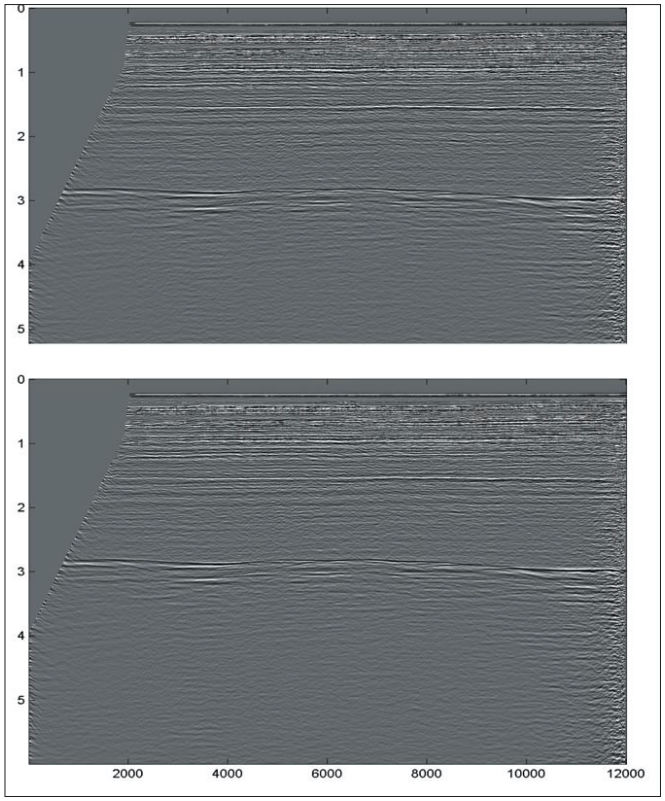

Figure 5. *North Sea stacks. First pass (upper panel) and second pass (lower panel).*

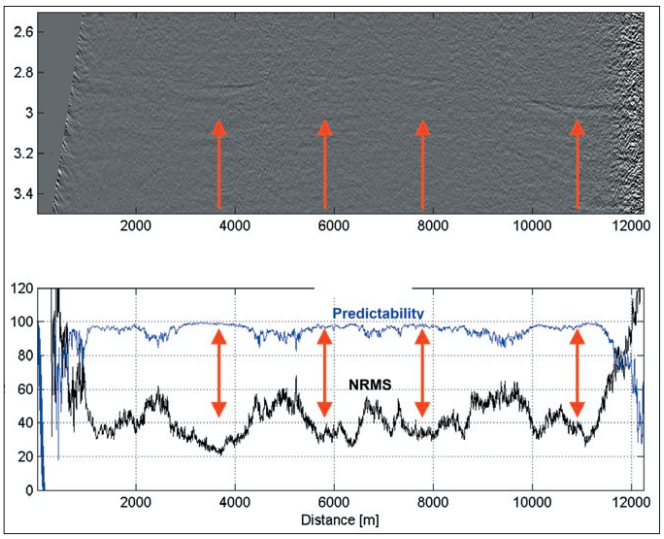

Figure 6. *North Sea data. Difference image (upper panel), nrms and predictability values (lower panel). The red arrows indicate where visually less repeatable seismic correlates with lower values of nrms and higher values of predictability.*

Data example 2, North Sea. The second data example is a single 2D line taken from the central streamer of a repeat swath of six streamers acquired in the North Sea during 2001. Data were acquired from point receivers and processed using digital group forming. The output group interval was 6.25 m. Both lines were processed identically. Active streamer positioning control was used when acquiring these data, and positioning repeatability was extremely high. In-line positioning errors for source and receivers are within 3 m and 5 m, respectively. Cross-line positioning errors are within 5 m and 30 m (source and receivers), and are generally less than this with an rms midpoint error of around 5 m.

Figure 5 shows the first pass (line 034, upper panel) and second pass (line 065, lower panel). No migration has been performed; the stacks are log-stretch DMO stacks. Figure 6 shows the difference image (upper panel) over the window 2.5-3.5 s obtained after subtracting the two processed stacked lines. The lower panel shows the nrms and predictability values (one for every CMP) computed from 2.5-3.5 s. The difference is, visually, highly repeatable over the whole line, though the nrms values are large, ranging from 20% to over 60% in places, with corresponding predictability values of over 99% to around 85%. Where the data are most predictable (over 99%), the corresponding nrms residual is just over 20% (exactly as in the Gulf of Mexico example). The negative correlation between the metrics is, again, also clear.

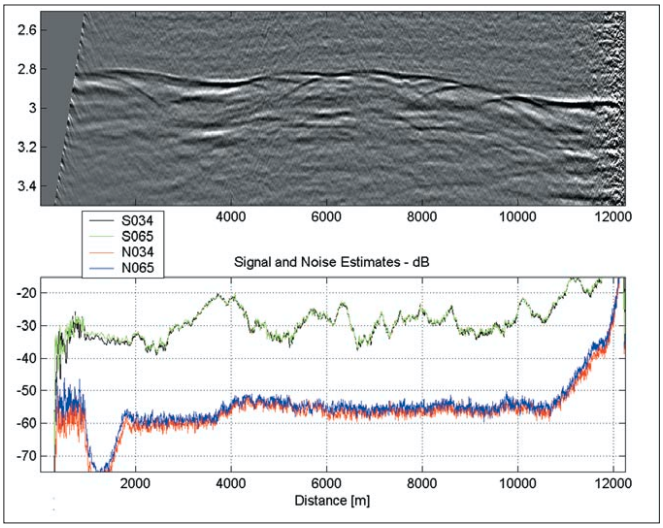

Figure 7. *North Sea data. First pass (upper panel) with signal and noise estimates in dB (lower panel).*

The high values of nrms are surprising, given that the data are visually very repeatable. The large range in the repeatability metrics is also interesting. We note that this does not correlate with the acquisition geometry in any way. Visually, from Figure 6, the fluctuations in nrms and predictability appear to inversely correlate with the seismic repeatability; where there is greater residual signal (as marked by the red arrows), the nrms values are smallest (largest predictability). Conversely, the largest nrms values (smallest predictability) appear to correlate with areas of less residual signal. This is not what we expect from our repeatability metrics, as we would like these to be a measure of the seismic repeatability.

Signal and noise estimates were computed for both lines from 2.5 s to 3.5 s. The signal estimate was computed from the zero lag of the cross-correlation between neighboring CMPs, and the noise estimate was computed from the zero lag of the average auto-correlation of the two CMPs, minus the signal estimate. This method estimates the uncorrelated noise and assumes that the signal does not change across neighboring CMPs. This is a reasonable assumption given the small CMP interval of 3.125 m. We note that because the data are unmigrated stacks, diffraction energy will partly contribute to this noise estimate.

Figure 7 shows the signal and noise estimates below the first pass line 034. The values are plotted in dB with respect to the peak signal level. The black line is the signal estimate for line 034 and the green line is for the second pass, line 065. They are very similar. The red line is the noise estimate for 034 and the blue line is for 065. They are, again, very similar. Although there is some mild correlation between the signal and noise estimates, the signal is generally fluctuating the more with the noise at a more constant level along

the line. This implies the noise is not purely due to perturbations because the noise would then be at a fixed level below the signal.

Figure 7 shows that there are a number of places where the noise level does change. To the left of the 4000-m mark, the noise level drops slightly on both passes. We have no explanation for this. However, the significant noise reduction to the left of 2000 m (and which is observable in the seismic image) correlates with the position of the first shot. To the left of this, increasingly fewer near offsets contribute to the stack. At the very left edge, the noise increases again where the fold of stack progressively decreases. The opposite effect is observed on the right of Figure 7. The noise rapidly increases after the point where we lose the far offsets from the stack (to the right of the 10 000-m mark). These observations imply that the noise is present on the near offsets to a greater degree, which might be expected. However, it is believed caused by the DMO operator—the noise-attenuating effect of the DMO operator is a function of offset because the operator aperture increases with offset. This is a subject for further investigation.

From the signal and noise estimates, we compute the noise-to-signal ratio, and we average the values from both lines as they are so similar. Figure 8 shows the same difference image and repeatability metrics as Figure 6, but with the noise-to-signal ratio also shown (red curve). The correlation with the repeatability metrics is startling. Clearly, fluctuations observed in nrms (or predictability) have little to do with signal "repeatability" but directly relate to the noise-to-signal ratio in the data, before any differencing. Because the noise level is relatively constant compared to the signal level (Figure 7), the repeatability metrics are simply showing the seismic signal strength.

The correlation of nrms with the noise-to-signal ratio (N2S) is explainable. Nrms equals the rms of the difference between the two repeat lines (the time-lapse noise) divided by the average rms of the signal and noise in the two lines. For small noise values, nrms is approximately the rms of the time-lapse noise divided by the rms of the signal. The noise-to-signal ratio is the mean square of the noise divided by the mean square of the signal. If the noise is purely random, then the time-lapse noise rms amplitude equals $\sqrt{2}$ times the noise in either input trace. We then end up with the relationship:

$$N2S = \frac{NRMS^2}{2} \quad \text{for random noise and noise << signal.}$$

This will not be an exact relationship with real data as there is residual signal and the noise is not random or, necessarily, small. However, the observed correlation between nrms and N2S tells us that noise-to-signal ratio is driving the repeatability metrics.

Synthetic example. Figure 9 shows a simple synthetic example. The data are composed of a single trace replicated a number of times with a fixed time window scaling down the amplitudes by 0.6 and to zero over a portion of the trace. The few traces to the right are all zero valued. Data in the top left panel represent the baseline survey, and data in the bottom left panel represent the repeat survey. All we have done is scale the amplitudes by 0.9 for the repeat survey (for example, a simple approximation to a source strength difference). The difference data are shown in the panel to the top right. The panel to the bottom right shows the repeatability metrics nrms and predictability. Predictability is 100% for the whole line and nrms is constant (about 10.5%) for the whole line. Data are noise free.

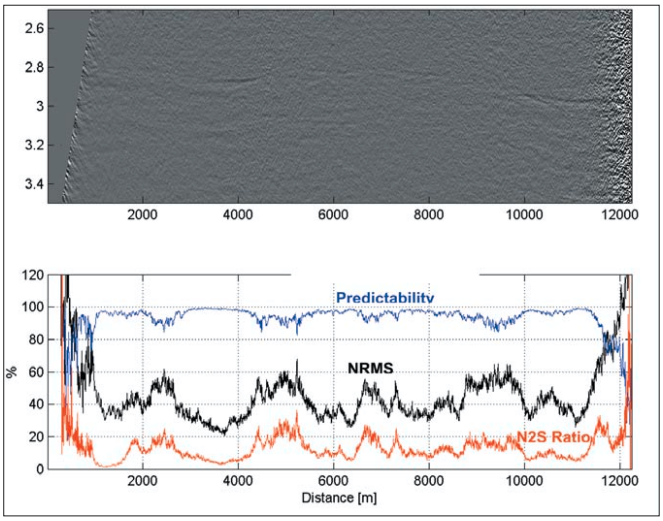

Figure 8. *North Sea data. Difference image (upper panel), nrms and predictability values (lower panel), as shown in Figure 6, with the average noise-to-signal ratio plotted in red.*

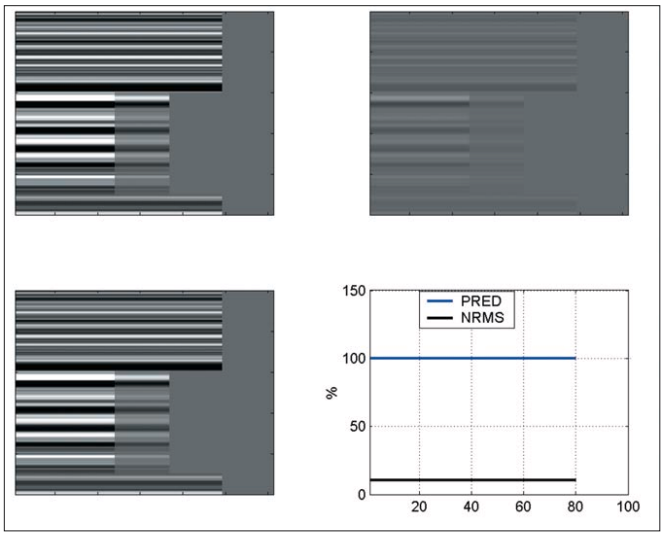

Figure 9. *Synthetic data, noise free. Baseline (top left), repeat (bottom left), difference (top right), repeatability metrics nrms and predictability (bottom right).*

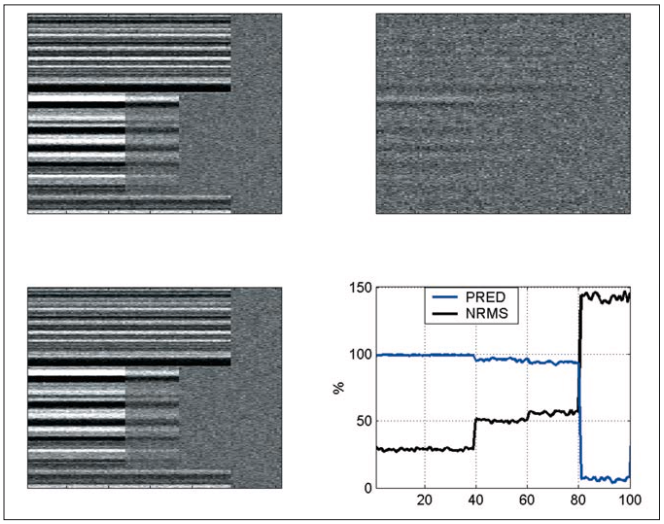

Figure 10. *Synthetic data with added white noise. Baseline (top left), repeat (bottom left), difference (top right), repeatability metrics nrms and predictability (bottom right).*

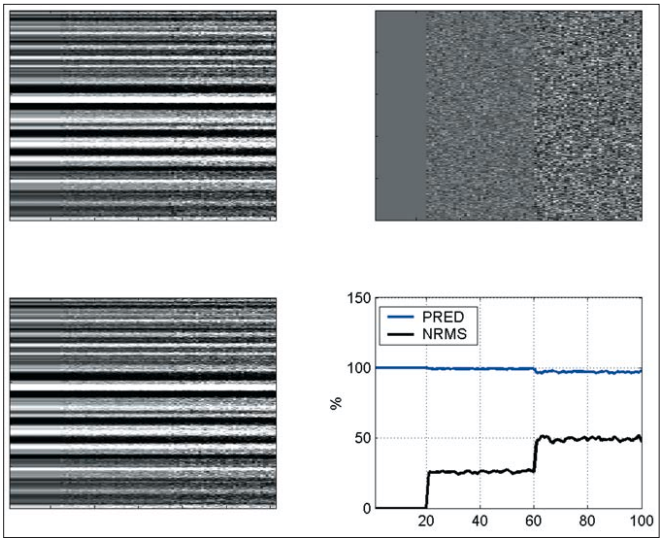

Figure 11. *Synthetic data with constant signal and increasing noise levels. Baseline (top left), repeat (bottom left), difference (top right), repeatability metrics nrms and predictability (bottom right).*

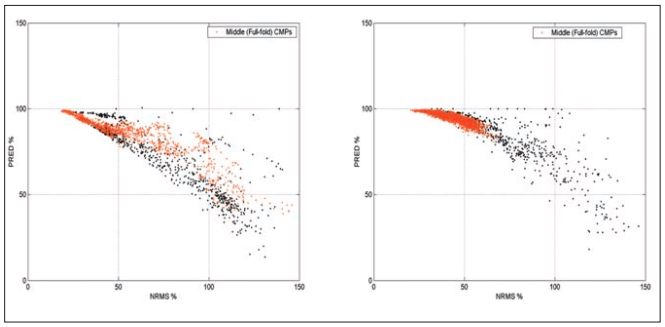

Figure 12. *Nrms predictability crossplots. Gulf of Mexico data (left), North Sea data (right).*

Figure 10 shows exactly the same synthetic example but with white noise added to both the baseline and repeat survey. The standard deviation of the white noise is 5% of the peak signal amplitude. The effect on the repeatability metrics (bottom right) clearly demonstrates what is happening in the real data; the repeatability metrics are directly related to the signal-to-noise level, and because the noise level is constant, they relate directly to signal strength. For the zero signal strength traces on the far right, nrms values are around 141% and predictability values are near zero (theoretically zero for truly random noise).

The synthetic results suggest that nrms is more sensitive to changes in the signal-to-noise level than predictability (at these high values of predictability). This is what we observed on the real North Sea data example (Figures 6 and 8). However, because the noise level is constant in this synthetic example, the varying signal level may be biasing this observation. The following final synthetic example demonstrates the effect of varying noise levels. In Figure 11, the signal is constant for all traces. 5% white noise has been added to the central traces, and 10% white noise has been added to traces to the right (the standard deviation of the white noise is related to the peak signal amplitude). The repeat data set is simply the same with different seeds for the noise generation. The metrics (bottom right) clearly show that nrms is more sensitive to changes in the noise level than predictability is, for these high levels of predictability; we note that, for typical repeat seismic data, predictability values will generally be quite high.

Repeatability or predictability? From the Gulf of Mexico data example, it appears that the streamer position repeatability governs data repeatability; this appears to be the overriding factor. From the North Sea data example, it appears that signal-to-noise governs data repeatability, the data acquisition geometry being highly repeatable. In both cases, there seems to be a relationship between the repeatability metrics, nrms and predictability. As we have already noted, nrms is very sensitive to any change in the data or noise, whereas predictability is sensitive to reflectivity changes and to noise. Either metric used alone can be misleading. In this section, we examine plots of the predictability and nrms values to gain an insight into their relationship.

Figure 12 shows plots of predictability and nrms for the real data examples, Gulf of Mexico (left) and North Sea (right). The negative correlation between the metrics is clear and, in both cases, there is a sharp bounding edge to the lower left of the cross-plot values. Data points in red are for the central full-fold traces, which tend to lie toward the top left of the plot (more repeatable data).

The sharp bounding edge is intriguing and some simple modeling suggests an explanation, the results of which are shown in Figure 13 (left panel). Two initially equal traces were perturbed and the repeatability metrics were calculated for the resulting difference trace. Traces were perturbed in amplitude, static, and phase, and by adding increasing amounts of random noise to the traces. Amplitude, static, and phase perturbations result in the expected straight line parallel to the abscissa; predictability is not sensitive to these changes. Random noise perturbations result in a bell curve similar to the bounding edge of the real data plots (Figure 12). At the peak of the bell, a large change in nrms corresponds to a small change in predictability, supporting the assertion that nrms is sensitive to small perturbations at high repeatabilities (also observed in our modeling examples). As we move down this curve, data are less correlated; at 141% ($\sqrt{2}$) nrms and 0% predictability, the data are completely uncorrelated. Where there is a combination of these perturbations (as expected on real data) we would expect many points to lie to the right of this bounding line, as in the real data.

The relationship between nrms and predictability can be worked out theoretically for the random noise case. If the ratio of the white noise amplitude to initial trace amplitude is λ, then we obtain the following relationships, expressed as percentages:

$$NRMS = \frac{141}{\sqrt{1+\frac{1}{\lambda^2}}} \quad \text{and} \quad PRED = \frac{100}{(1+\lambda^2)^2}$$

To work out this relationship for predictability, we have considered only the zero lags of the correlations, whereas values of predictability presented in this report use 16 positive and 16 negative lags (as defined by the WesternGeco data processing software). The inclusion of more lags essentially dampens, or smoothes, the predictability computation (if all lags were considered predictability would always be 100%), and we can simulate this by adding a damping term, d, to the equation:

$$PRED = \frac{100}{(1+d\lambda^2)^2}$$

These theoretical curves are in the right panel of Figure 13 as plots of nrms and predictability. The blue curve is for the undamped case, and the red curve is for the damped case. The modeled points for the random noise perturbations, as shown in the left panel of Figure 13, are also plot-

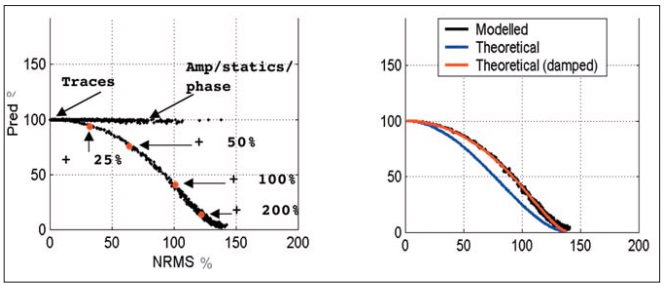

Figure 13. Nrms predictability crossplots. Synthetic modeled data (left), theoretical curves for random noise (right).

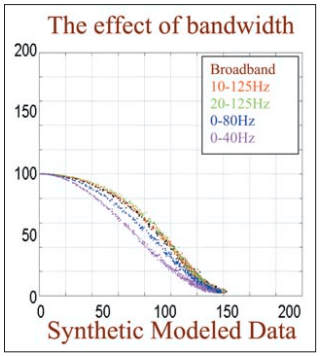

Figure 14. Nrms predictability crossplots. Synthetic modeled random noise data. Broadband (black) as shown in Figure 13. 10-125 Hz (red), 20-125 Hz (green), 0-80 Hz (blue), and 0-40 Hz (magenta).

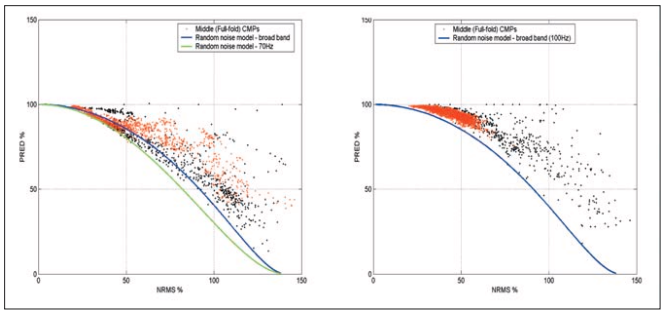

Figure 15. Nrms predictability crossplots, as shown in Figure 12. Gulf of Mexico data (left), North Sea data (right). The modeled curve for broadband random noise is blue. On the Gulf of Mexico data, the modeled curve for 5-70 Hz is green.

ted. The theoretical curves exhibit the bell-like shape seen in the real data and modeled data, and a value of d=0.75 seems to accurately represent the modeled points, i.e. d=0.75 compensates for the 16-lag smoothing of the predictability computation for the (broadband) random noise case.

The effect of bandwidth. The synthetic modeling was repeated using random noise, but after applying varying band-limiting filters. Figure 14 shows the resulting plots. The broadband results of Figure 13 are black, along with 10-125 Hz (red), 20-125 Hz (green), 0-80 Hz (blue), and 0-40 Hz (magenta). As the low end is cut, there is a slight increase in predictability with little change in nrms; hence, the curve shifts slightly up. As the high end is cut (which we might often expect on real data), predictability still slightly increases (it will always increase as the bandwidth is limited), but the overriding effect is a reduction in nrms; hence the curves shift to the left.

Figure 15 shows the real data plots (as in Figure 12) but with the modeled curves for random noise (which agree with theoretical curves for the broadband case) also plotted. Average noise spectra were computed for the two real data sets where there was least residual signal. The Gulf of Mexico data show the noise falling away after 70 Hz. The North Sea data show more broadband noise up to 125 Hz. In Figure 15, the blue curve is for broadband noise, and the green curve (left, GoM only) is for 5-70 Hz. The modeled curves show an excellent fit to the real data in both cases; the hard bounding edge appears to define the residual noise field, which will vary with the bandwidth and with the form of the noise.

A matching methodology. We make the assertion that the hard leading edge observed in the real data defines the random time-lapse noise field. Nrms is sensitive to amplitude, phase, and static change, whereas predictability is not; it reflects changes in the reflectivity and in the noise. Matching two data sets with linear filters should move points on the plot to the left, toward the leading edge, predictability is unaffected.

We suggest a matching methodology of (1) plotting predictability versus nrms, (2) identifying data that trail away from the leading edge of the plot, (3) using the sensitivity of nrms to minimize the perturbations in static, amplitude, and phase to bring the data back to the leading edge of the plot (the leading edge can be seen as representing the matching goal for nrms for a given noise level), (4) correlating nrms and noise-to-signal ratio; a positive correlation implies that noise is the dominating factor driving the metrics (5) application of noise reduction methods then move the data up this leading edge.

Discussion and conclusions. We have analyzed two different repeat seismic lines in terms of repeatability metrics, nrms, and predictability. The results are very different.

In one case, residual differences correlate with streamer position repeatability. Where the streamer positions closely coincide, data are highly repeatable, demonstrating that repeatability errors in the source position and source signature, after shot-by-shot signature deconvolution, are much less than those due to streamer position nonrepeatability. The nrms error correlates with CMP position error and is consistent with the results of Morice et al. (2000). No active streamer positioning was used during acquisition of these data.

In the second case, active streamer positioning was used during the acquisition and the positioning repeatability was very good. Data are highly repeatable along the whole line, though trace residuals are large (larger than in the first case), and the residual differences anticorrelate with the signal-to-noise ratio in the data. The background random noise level appears to be high (and fairly constant) in these data, and leads to the nrms error correlating with the signal strength. In this case (where noise is dominant), variations in nrms tell us nothing about the signal repeatability. This correlation of nrms with signal-to-noise ratio tells us that noise to-signal ratio is driving the repeatability metrics, not the signal repeatability.

The metrics of nrms and predictability alone do not lead to an intuitive understanding of the data repeatability, and they require interpretation of their values. We observe predictability values of 90-(almost) 100%, which suggest high repeatability, but corresponding nrms residuals of 60-18% suggest data that are not so repeatable. We also observe high nrms values when the data are, visually, highly repeatable. These observations may help to explain why Koster et al. (2000) distinguish water replacing oil in Draugen (an impedance change of 10%, but an unstated reflectivity change) with nrms of 35%. It may also explain why Kristiansen et al. (2000) observe a visually better repeatability on the Foinaven seabed data (predictability, 96%) than the towed data (predictability, 93%). We may also infer in the Foinaven case that the unpredictable power to total power ratios are 4% and

7%, respectively. Therefore, the seabed data have just over half the time-lapse noise power of the towed data. However, relying solely on predictability can be misleading, as it is insensitive to amplitude, static, and phase changes.

Plots of nrms and predictability values show a sharp bounding edge, which is interpreted as a reflection on the residual time-lapse noise field, which is bandwidth dependent. We note also that nrms is more sensitive to changes in random background noise when predictability values are high. These observations and sensitivity differences suggest a matching methodology of (1) plotting predictability and nrms; (2) identifying the data which trail away from the leading edge of the crossplot; (3) using the sensitivity of nrms to minimize the perturbations in static, amplitude, and phase to bring the data back to the leading edge of the crossplot (the leading edge can be seen as representing the matching goal for nrms for a given noise level); (4) correlating nrms and noise-to-signal ratio; a positive correlation implies that noise is the dominating factor driving the metrics, and (5) application of noise reduction methods then move the data up this leading edge.

Typically, noise reduction will occur prior to final signal matching as part of processing in order to optimize the signal-to-noise ratio in the final images. Because the data presented here are unmigrated stacks, the crossplot metrics reside lower down the leading edge than could be ultimately achieved.

The combination of repeatability metrics should assist in matching time-lapse data sets, but metrics of the prior uncertainty in the data, together with careful analysis during processing, are needed to assess overall uncertainty and repeatability of the two surveys and their relation to the time-lapse signal and to the signal-to-noise levels.

Suggested reading. "Marine seismic cable steering and control" by Bittleson et al. (EAGE 2000 *Expanded Abstracts*). "A proven concept for acquiring highly repeatable towed streamer seismic data" by Eiken et al. (EAGE 1999 *Expanded Abstracts*). "Signal preserving swell noise attenuation using point receiver seismic data" by Jenkerson et al. (SEG 2000 *Expanded Abstracts*). "Using legacy seismic data in an integrated time-lapse study: Lena Field, Gulf of Mexico" Johnson et al. (*TLE*, 2000). "Time-lapse seismic surveys in the North Sea and their business impact" by Koster et al. (*TLE*, 2000). "Seismic repeatability, normalized rms and predictability" by Kragh and Christie (SEG 2001 *Expanded Abstracts*). "Foinaven 4D: processing and analysis of two designer 4Ds" by Kristiansen et al. (SEG 2000 *Expanded Abstracts*). "The impact of positioning differences on 4D repeatability" by Morice et al. (SEG 2000 *Expanded Abstracts*). "Adaptive beamforming with generalized linear constraints" by Özbek (SEG 2000 *Expanded Abstracts*). "Partial coherence matching of synthetic seismograms with seismic traces" by White (*Geophysical Prospecting*, 1980). TLE

Acknowledgments: We thank the many colleagues at WesternGeco who were involved with this work. However, the responsibility for errors remains with us.

Corresponding author: edkragh@slb.com; pafc1@slb.com